Aggrandized catalytic and bactericidal activity of silver and polyvinylpyrrolidone capped bismuth oxybromide quantum dots: *In silico* molecular docking studies

Muhammad Shahid Yousaf[a], Ali Haider[b], Anum Shahzadi[c], Anwar Ul-Hamid[d], Muhammad Imran[e], Muhammad Ali Khan[a]*, Walid Nabgan[f], Murefah mana Al-Anazy[g], E. El Shiekh[h], Muhammad Ikram[i]*

[a]Institute of Chemical Sciences, Bahauddin Zakariya University Multan, 60800, Pakistan
[b]Department of Clinical Sciences, Faculty of Veterinary and Animal Sciences, Muhammad Nawaz Shareef, University of Agriculture, Multan 66000, Punjab, Pakistan
[c]Faculty of Pharmacy, The University of the Lahore, Lahore 54000, Pakistan
[d]Core research facilities, King Fahd University of Petroleum & Minerals, Dhahran 31261, Saudi Arabia
[e]Department of Chemistry, Government College University, Faisalabad, Sahiwal Road, Sahiwal, Punjab, 57000, Pakistan
[f]Departament d'Enginyeria Química, Universitat Rovira i Virgili, Av Països Catalans 26, 43007 Tarragona, Spain
[g]Department of Chemistry, College of Sciences, Princess Nourah bint Abdulrahman University (PNU), P.O. Box 84428, Riyadh, 11671, Saudi Arabia
[h]Department of Radiological Sciences, College of Applied Medical Sciences, King Khalid University, Abha, 61421, Saudi Arabia
[i]Solar Cell Applications Research Lab, Department of Physics, Government College University Lahore, Lahore 54000, Punjab, Pakistan

Corresponding author's email: dr.muhammadikram@gcu.edu.pk (M. Ikram), malikhan@bzu.edu.pk (M. Ali Khan)

ABSTRACT

The current study reports a novel synthesis of bismuth oxybromide (BiOBr) quantum dots (QDs) doped with different concentrations (3 and 6 wt. %) of silver (Ag) and a fixed amount of polyvinylpyrrolidone (PVP). This research investigated the catalytic and antibacterial activity with evidential molecular docking analysis of Ag/PVP doped BiOBr QDs. The Ag and capping agent (PVP) were added to BiOBr as they regulate the growth of QDs and prevent their agglomeration that caused to increase in the catalytic and antibacterial activity. These binary dopants-based BiOBr QDs can be an ideal catalyst for disintegrating methylene blue dye and a potential inhibitor against the multiple drug resistance (MDR) *Escherichia coli* (*E. coli*) pathogen. Notably, 6% Ag/PVP doped BiOBr showed a significant catalytic reduction of methylene blue (MB) in a basic medium (pH~12) compared to other environments. The results of the molecular docking investigation suggested that Ag/PVP-doped BiOBr QDs might be

inhibitors of FabH and deoxyribonucleic acid (DNA) gyrase from *E. coli*, which was consistent with their *In vitro* antimicrobial activity.

Keywords: Quantum dot; antibacterial activity; catalytic activity; BiOBr

1. INTRODUCTION

Water is an integral component of life and is significant in industry and the planet's productivity. The dangerous contaminants (heavy toxic metals and pigments) threatened by aquatic life are excreted into the water due to growing human pursuits and rapid industrial growth [1,2]. According to estimates, 7×10^5 tons of dyes are generated annually worldwide, and at least 25% are currently released into water bodies. Some organic dyes can cause skin problems and carcinogenesis, leading to cancer and other disorders [3]. According to the spatial arrangement of ionic charges, dye molecules are often categorized as anionic, cationic, or non-ionic. Cationic dyes exhibit more cytotoxic effects than anionic dyes [4]. Methylene blue (MB), a cationic dye with a heterocyclic aromatic structure, was used as a staining agent in the body tissue and different industries, including paper, hair, and cotton. Medical professionals also employ methylene blue to treat cyanide poisoning [5]. Despite its more comprehensive applications, this dye causes many risks to living things. Methylene blue causes nausea, vomiting, diarrhea, gastritis, excessive perspiration, eye burns, respiratory problems, increased heart rate, chest pain, jaundice, headache, cyanosis, and tissue necrosis [6]. Several removal techniques have addressed this environmental concern that can successfully degrade such toxic chemicals from the aqueous medium. Adsorption [7], chemical reduction [8], membrane filtration [9], photo-oxidation [10], ion-exchange removal [11], catalytic ozonation [12], biological (aerobic/ anaerobic) therapies [13], and catalytic activity [14] are some of the removal techniques. Among these, photocatalysis and catalysis are considered advantageous for the environment, economically feasible and

exceptionally effective in completely oxidizing and mineralizing dangerous organic material [15,16]. Cow mastitis is a bacterial infection or physical stress-related inflammation of the glandular mucosa of the mammary gland. It is said to be the most common illness that costs maximum since the amount and quality of milk have decreased [17]. Several risk factors, including host, environment, and pathogens like *E. coli*, are thought to impact the incidence of bovine mastitis [16] substantially. Antibacterial effects of metal nanoparticles have been seen because of their tiny size and large surface-to-volume ratio, which enables them to bind intimately with bacterial membranes [18]. Nanomaterials (NMs) have excellent adsorption capacity, reactivity, and solid catalytic activity, which may be due to their compact size and highly specified surface area. NMs of wide varieties have been utilized to successfully remove organic wastes, including heavy metal ions, inorganic anions, and numerous types of bacteria [19,20]. Bi-based semiconductors, including Bi_2O_3, Bi_2S_3, Bi_2WO_6, and BiOX (X = Cl, Br, and I), continually get enhanced concentration due to their potential use in degradation [21,22]. BiOBr is preferred because of its high stability, indirect transition band gap energy (E_g), layered structure, and efficient pollutants degradation [23–25]. Compared to other adsorbents, BiOBr low adsorption capability means it can't be used in many industrial water purification processes [26]. According to various studies, introducing PVP increased the adsorption capability of BiOBr [26]. PVP's superior stability, non-toxicity, steric action, and bio-compatibility have made it an attractive choice as a capping agent in the production of catalysts [27]. PVP is a promising option for enhancing the activity of catalysts by modifying nanocrystals through chiral modification, charge carrier transfer enhancement, and adsorption adjustment [42]. Metal doping has gained widespread attention as a classic approach to nanomaterial modification due to its ease of use, the versatility of doping elements, and the simplicity of functionalization after modification.

Introducing inorganic metal nanomaterials such as Pt, Au, Ag, Zn, Co, and Ni has been a widely employed strategy to increase catalytic activity over the years [23,28,29]. Especially, Ag has received considerable attention due to its significant antibacterial and dye elimination action due to its large surface-to-volume ratio [30,31]. The novelty of this project is low temperature, open-air facile synthesis of co-precipitated BiOBr QDs capped with polymer (PVP) and transition metal (silver). The capping of binary dopants (Ag and PVP) to BiOBr inhibit the growth, agglomeration and recombination rate of QDs, resulting in the enhanced catalytic reduction of MB and antibacterial activity.

The current research adopted the co-precipitation technique to prepare BiOBr doped with PVP and (3 and 6 wt. %) Ag. The synthesized QDs were used for the catalytic de-colorization of MB and antibacterial potency against *E. coli.*

2 EXPERIMENTAL SECTION

2.1 Materials

$Bi(NO_3)_3.5H_2O$ (98%) was retrieved from BDH Laboratory Supplies (England). NaOH (98%), PVP, and silver nitrate ($AgNO_3$ 99.8%) were acquired from Sigma-Aldrich. Potassium bromide (KBr, 98%) was sourced from Uni-Chem.

2.2 Synthesis of Ag/PVP-doped bismuth oxybromide

0.7M $Bi(NO_3)_3.5H_2O$ (Solution 1) and 0.7M KBr (Solution 2) were dissolved under vigorous agitation and heated at 100 ^oC for 10 min. After strring, solution 2 was poured into solution 1 dropwise, and the pH~12 was maintained by adding 0.7 M of precipitating agent (NaOH). The obtained solution was centrifuged at 7000 rpm for 8 min to achieve metal hydroxide and

eliminate contaminants. The washed sediments were vaporized at 150 ^{o}C for 12 h and crushed with mortar and pestle to obtain a fine powder. For doping, the fixed amount (2 wt. %) of PVP with different concentrations (3 and 6 wt. %) of Ag were doped in the above mentioned solution of BiOBr to prepare the ternary system.

2.3 Catalysis

Catalytic activity (CA) of BiOBr and (3, 6%) Ag/PVP doped BiOBr in different media was utilized to degrade the MB dye. The standard and loaded solutions (400µL) were added in aqueous MB (3 mL) to test the dye degradation by UV spectrophotometer in the range ~200-800 nm. $NaBH_4$ induced MB to transform into leucomethylene blue (LMB), confirming the dye degradation. The degradation rate (%) was calculated using degradation rate (%) = C_o-C_t/ C_o × 100, where C_o is the initial concentration of the MB in the solution, and C_t is the concentration that changes over time.

2.3.1 Catalysis mechanism:

The general mechanism for catalytic de-colorization of MB using a reducing agent ($NaBH_4$) is faster, simpler, easier to use, and recyclable than conventional methods. The main characteristics of the catalysis mechanism include the incorporation of a reductant and nanocatalyst within the dye. During catalysis, $NaBH_4$ acts as a reducing agent that gives an e^- to MB, an oxidizing agent. A redox reaction that results in the e^- transfer from $NaBH_4$ to MB causes the synthetic dye to degrade. The degradation efficiency was significantly less and time-consuming only in the presence of a reducing agent; adding nanocatalysts increased the reaction rate [32]. The decreased activation energy that caused a rapid redox reaction was reduced when a catalyst (pure and doped materials) was included. The attachment sites on the surface of QDs facilitated the

adsorption of the reduction agent ($NaBH_4$) and the substrate (MB). This adsorption is a quick and reversible phenomenon. QDs serve as an electron relay junction for the molecules that have been adsorbed and cause the reduction of MB (Fig. S1) [33].

2.4 Segregation and characterization of multiple drug resistant (MDR) *E. coli*

Bovine lactation specimens were procured from several livestock facilities in Pakistan and first tested using a surf-field mastitis test. To ascertain Gram-negative (G -ve) *E. coli* bacteria, the specimens were cultivated on 5% sheep blood agar, which resulted in the development of colonies. MacConkey agar was used in triplicate to purify the established strains of *E. coli* further. Isolated *E. coli* was tested for antibiotic resistance using a disc diffusion assay on Muller Hinton agar (MHA), and any strain that showed resistance to three or more drugs after being incubated for 24 hours at 37°C was classified as multidrug-resistant (MDR). The diverse microbial populations were evaluated using biochemical (catalase and coagulase) and morphological (gram staining) methods.

2.5 Antimicrobial Activity

The bactericidal efficacy of pure and doped nanomaterials was evaluated by well diffusion technique by swabbing 0.5 MacFarland Gram-negative (G -ve) MDR *E. coli* pathogens on MA plate. Utilizing a sterilized cork borer, 6 mm diameter wells were drilled on MA plates. Different concentrations (500 and 1000 µg/50 µL) of Ag/PVP-BiOBr QDs were injected into each well under sterile conditions, and the results were compared with ciprofloxacin (5 µg/50 µL) and DI water (50 µL) as positive and negative standards, accordingly. The specimens' bactericidal property was determined following 24 hours of colonization at 37 °C by quantifying the inhibition area (mm) using a Vernier caliper.

2.7 Molecular docking analysis

The enzyme-binding affinity of both PVP-doped BiOBr and Ag/PVP-doped BiOBr QDs was studied. Owing to the better antibacterial properties of synthesized QDs against *E. coli*, we discovered and investigated the FabH and DNA gyrase from *E. coli* and their binding affinity within their dynamic pocket. The three-dimensional structures of chosen enzyme substrates were downloaded from the protein information database using the identification numbers 4Z8D (resolution: 2.0 Å) [34] and 6KZX (resolution: 2.1Å) [35] for $FabH_{E.\ coli}$ and $DNA\ gyrase_{E.\ coli}$, correspondingly. To perform the docking analysis, SYBYL-X 2.0 was adopted. Parallel to our previous research, we exploited SYBYL-X 2.0 to build three-dimensional frameworks of molecules and scrutinize QDs' binding interactions with the residues at specific interaction sites in specific proteins[36–38].

3 RESULTS AND DISCUSSION

Synthesis of BiOBr and (3, 6%) Ag/PVP-doped BiOBr QDs through the co-precipitation process (Fig. 1).

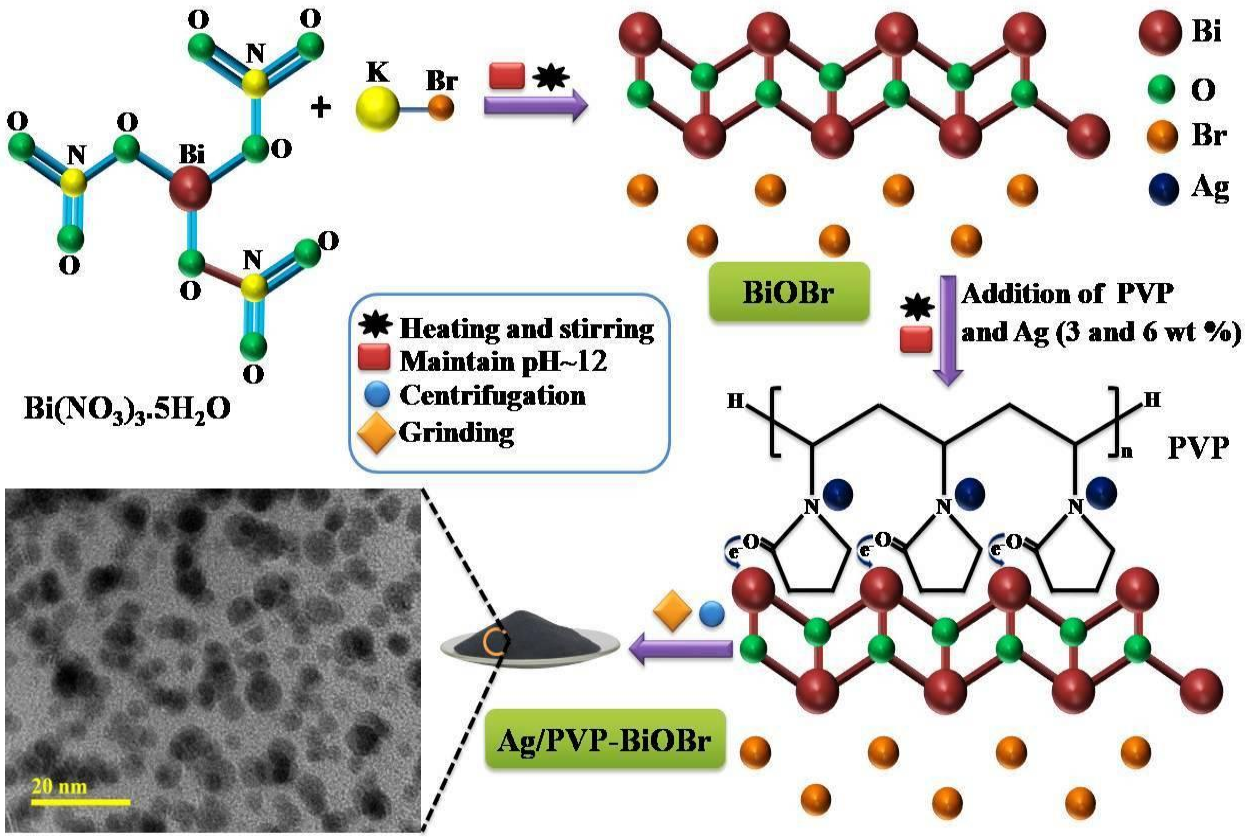

Fig. 1: Schematic illustration to synthesize BiOBr and Ag/PVP-doped BiOBr QDs by co-precipitation method

The structural properties of BiOBr and Ag/PVP doped QDs were analyzed by XRD, 2Θ ranging from 20 to 60° as presented in Fig. 2(a). Diffraction peaks sited at 25.48° (101), 29.21° (116), 31.73° (102), 44.88° (004), 46.46° (113), 51.52° (202), 56.16° (114) and 58.47° (203) revealed the tetragonal phase of BiOBr (JCPDS: 01-085-0862/96-201-6341) [39]. The addition of PVP showed that intensity of the peaks was reduced, which was assigned to enlargement in structural instability of BiOBr [40]. The incorporation of Ag into a binary system (PVP-BiOBr), a slight shifting of peaks toward a lower angle was observed, attributed to an increase in the d-spacing value. The crystallite size of BiOBr QDs was reduced 9.18-8.99 nm by adding PVP. Upon metal

doping (Ag) into binary system (PVP-BiOBr), the crystallite size was enhanced (8.99-9.02 nm). As crystallite size of BiOBr decreased gradually upon doping, the surface area increased, improving the catalytic reduction of MB. To ascertain the functional group composition and vibrational modes present in the BiOBr was confirmed by FTIR (Fig. 2b) [41]. The transmittance bands found at 3500 and 1630 cm^{-1} were attributed to O-H stretching and bending vibrations of adsorbed water, respectively [42,43]. The band appeared at 519 cm^{-1}, assigned to Bi-O stretching vibration [44–46]. The tensile displacement of the C-N heterocyclic band in PVP is attributed to the 1360 cm^{-1} band in the PVP-BiOBr transmission spectrum [47]. No additional band and prominent shift was observed in FTIR spectra after the incorporation of Ag. Furthermore, SAED pattern revealed bright circular rings of BiOBr and Ag/PVP-BiOBr QDs, indicating the samples are highly crystalline (Fig. 2c-e). As disclosed by XRD results, the crystallinity of BiOBr was diminished by PVP addition.

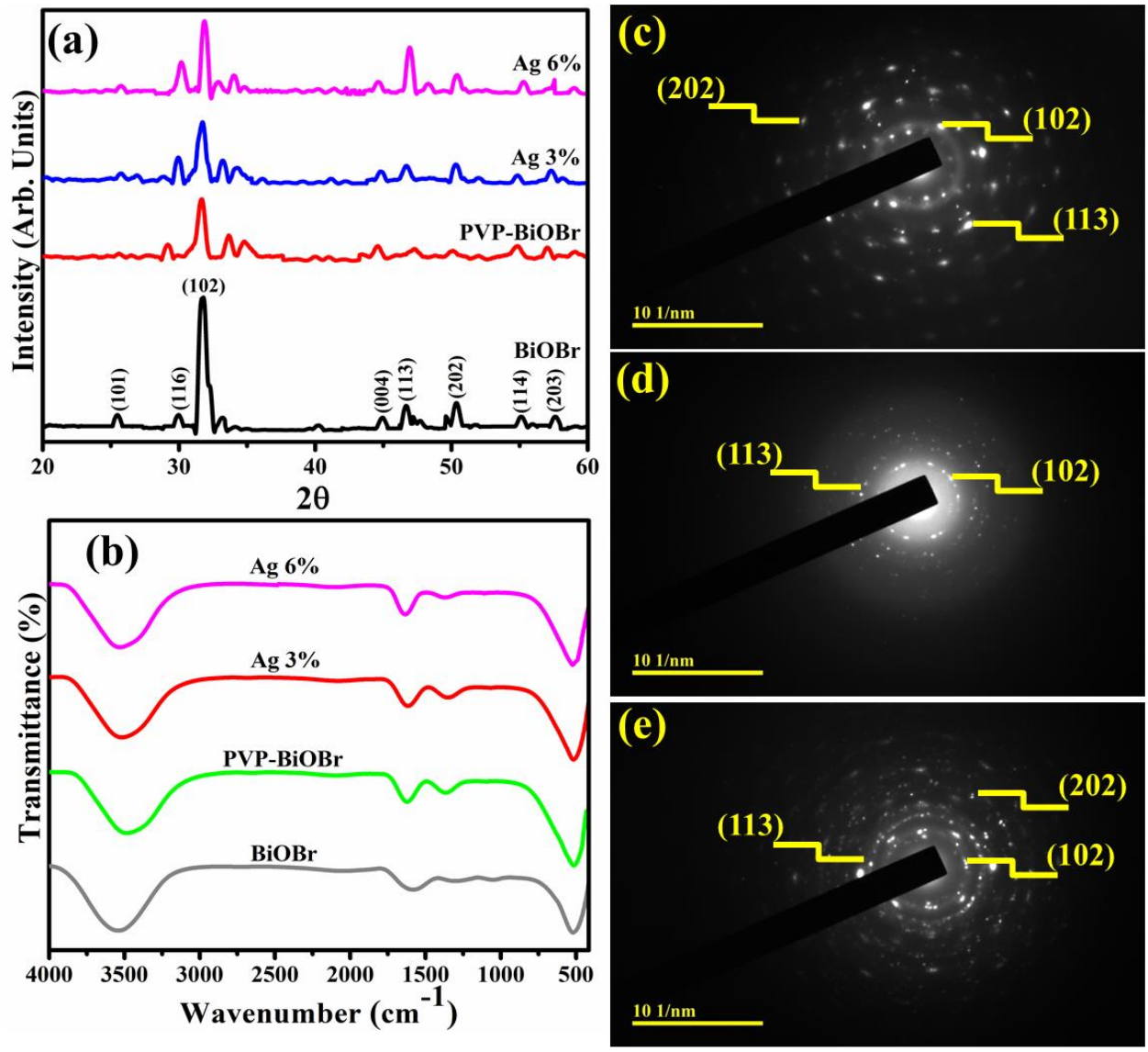

Fig. 2: (a) XRD pattern ,(b) FTIR spectra of BiOBr, PVP-BiOBr, 3% Ag/PVP-doped BiOBr and 6% Ag/PVP-doped BiOBr, and (c–e) SAED images of BiOBr, PVP-BiOBr and 3% Ag/PVP-doped BiOBr

The optical features of the BiOBr and Ag/PVP doped BiOBr were determined by UV-Vis spectroscopy, wavelength range from 230 to 500 nm (Fig. 3a). The synthesized BiOBr sample showed a considerable absorption peak around 315 nm [48]. The absorption decreased with Ag and PVP doping in BiOBr, introducing a hypochromic shift, suggesting the quantum

confinement effect [49]. Tauc's equation was used to measure the E_g of BiOBr, which increased from 3.69 to 4.12 eV upon doping of (3, 6%) Ag and PVP (Fig. 3b). This increase in E_g with Ag/PVP is correlated with crystallite size which decreased as mentioned above in XRD outcomes.

PL spectroscopy was utilized to explore the charge transfer efficacy of BiOBr and (3 and 6 wt. %) Ag/PVP doped BiOBr (Fig. 3c). The control sample (BiOBr) QDs showed a strong emission peak around 560 nm [50] and decrease in peak intensity for the PVP-BiOBr was noted, indicating that the electron-hole pair's recombination rate effectively reduced and charge transfer efficiency increased. The reduced emission peak intensity was attributed to the surface trap-induced emission because of the PVP capping [51]. Doping of Ag (3, 6 wt %) in the PVP-BiOBr lowers the peak intensity and enhances electron transit effectiveness by minimizing exciton interaction will boost the efficacy of catalytic activity.

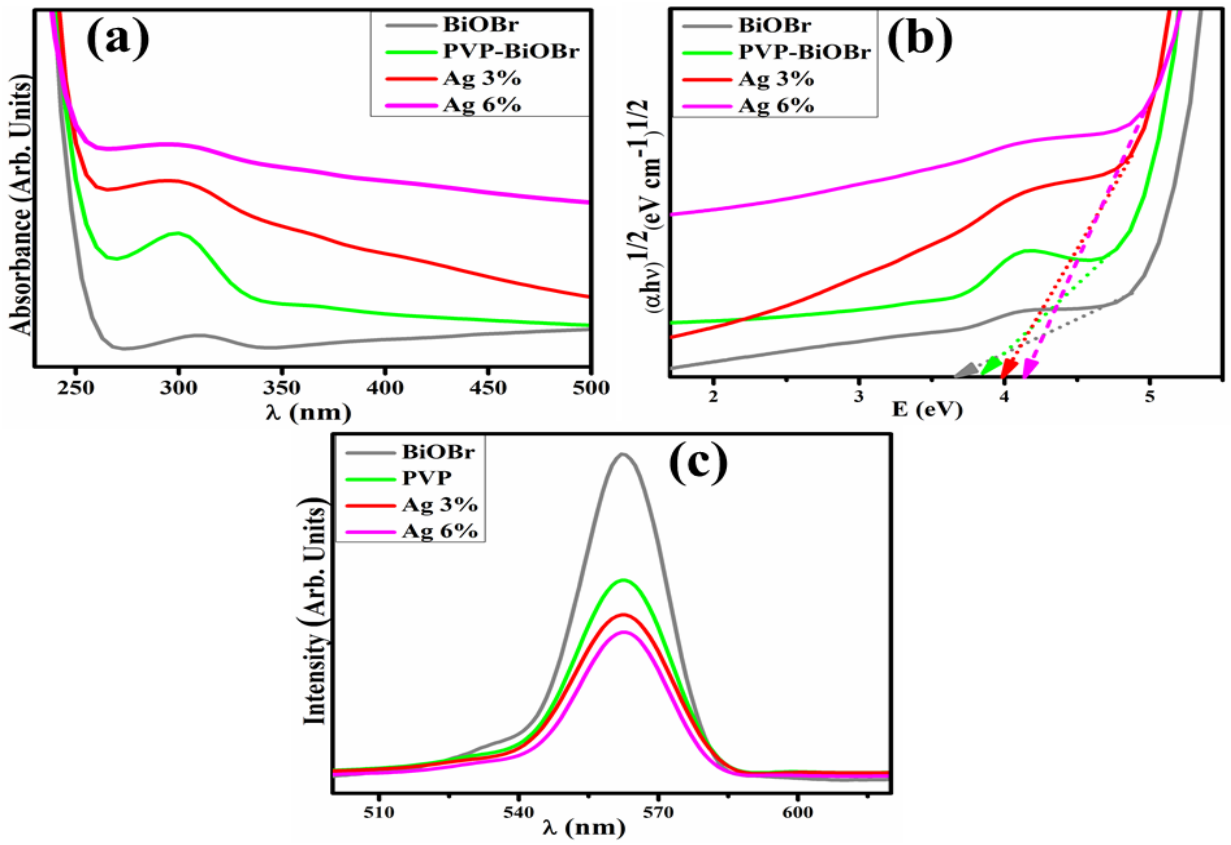

Fig. 3: (a) Electronic spectra (b) Tauc plot for Eg (c) PL emissions of pure and Ag/PVP-doped BiOBr QDs.

The element content confirmations of BiOBr and Ag/PVP-doped BiOBr have been determined using EDS (Fig. S2(a-d)). Bi, O, and Br peaks were observed, confirming that BiOBr and Ag peaks occurred due to doping. Potassium (K) peak appeared in specimens ascribed to the precursor employed in the synthesis process. Furthermore, using NaOH to stabilize the specimens' pH resulted in generating a Na peak. The Au was observed in the spectra due to the gold (Au) coating sprinkled on the sample to reduce the influence of charging. Due to operator error, the Ytterbium (Yb) peak appeared in the EDS spectra of BiOBr. To ensure the attainment of optimal interfacial contact configurations, EDS mapping was performed on higher-doped BiOBr to examine the dispersion characteristics of its constituent elements (Fig. S3). The six

identified elements (Bi, O, Br, Ag, Na, and K) were uniformly distributed across specimen levels with various elemental concentrations indicated by distinctive shades. Na, Au, and K were already described above as the contaminant, the specimen holders, and the precursor employed during the synthesis.

The structural morphology of BiOBr and Ag/PVP doped BiOBr has been confirmed by TEM analysis, Fig. 4(a–d). The development of the undoped BiOBr QDs clusters can be seen in Fig. 4(a). Upon doping of PVP, the BiOBr QDs seem to be covered by wafers of capping agent PVP (Fig. 4b). The addition of Ag to PVP-BiOBr showed the dispersion of spherical particle of Ag on the surface of binary system (Fig. 4c). Ag with higher concentration to PVP-BiOBr showed that Ag is attached with wafers wrapped QDs on the surface as well as at the interfaces (Fig. 4d). Furthermore, HRTEM were analyzed using Gatan software to calculate interlayer d-spacing information (Fig. S4a-b). BiOBr and 6 % Ag/PVP-doped BiOBr QDs d-spacing values were determined to be 0.292 and 0.293 nm, synchronized with XRD results.

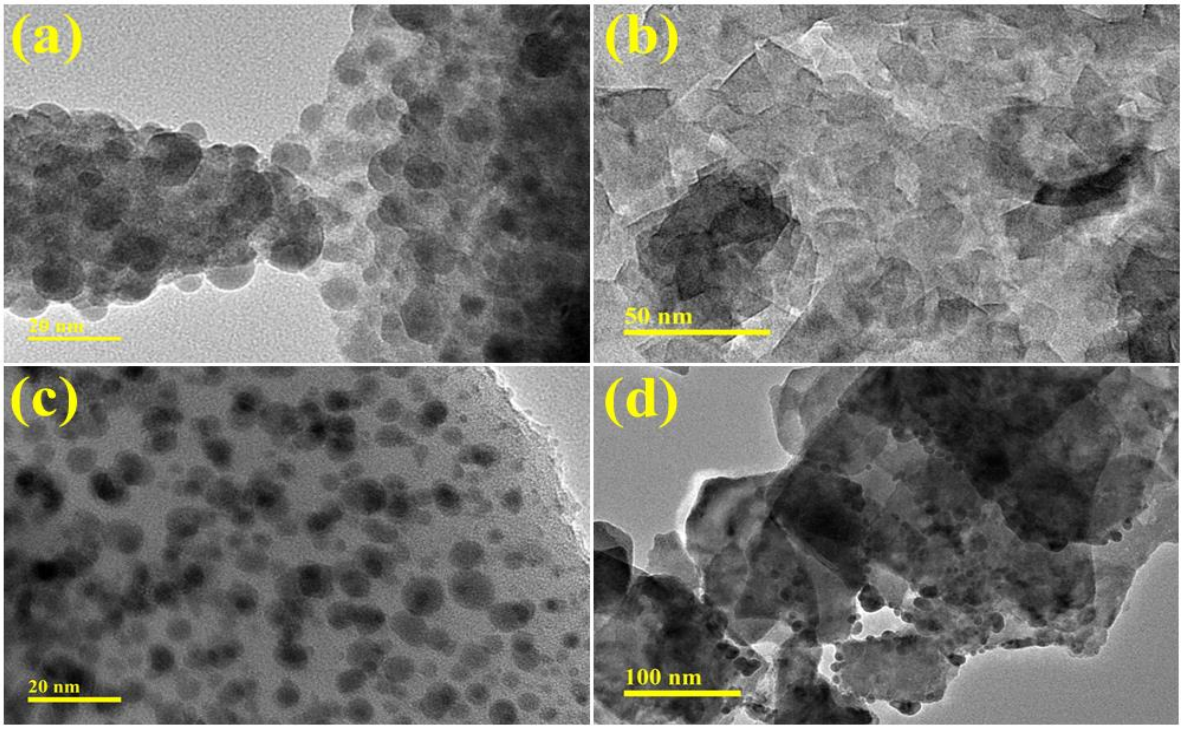

Fig. 4: TEM images of (a) BiOBr and (b) PVP-doped BiOBr (c) 3% Ag/PVP-doped BiOBr and (d) 6% Ag/PVP doped BiOBr QD

The catalytic activity of pure and (3, 6 wt. %) Ag/PVP doped BiOBr QDs were examined for the MB dye deterioration at different ranges of pH values (acidic, neutral, and basic media) in the presence of $NaBH_4$ using a UV-Vis spectrophotometer (Fig. 5a-c). The amount to which dyes degrade depends strongly on the pH of fluids, and CA of prepared catalysts is pH dependent. The pure and doped BiOBr revealed the maximum degradation of 48.81, 67.83, 80.74 and 83.77 % in neutral medium (pH=7), 37.48, 51.18, 73.88 and 98.75% in acidic medium (pH=4), 30.16, 33.5, 66.95 and 99.5% in basic medium (pH=12). Nanomaterials' crystallite size, morphology and surface area are highly dependent on catalytic activity. In this experiment, 6% Ag/PVP doped BiOBr exhibited the most significant catalytic activity throughout all media. Improvements in QDs' morphology contributed to this work's improved catalytic effectiveness for all mediums by

enhancing surface areas for reactions and surface-to-volume ratio shown by a drop in particle dimensions [52]. The comparison of catalytic activity of Ag/PVP doped BiOBr with literature has been demonstrated in Table 1.

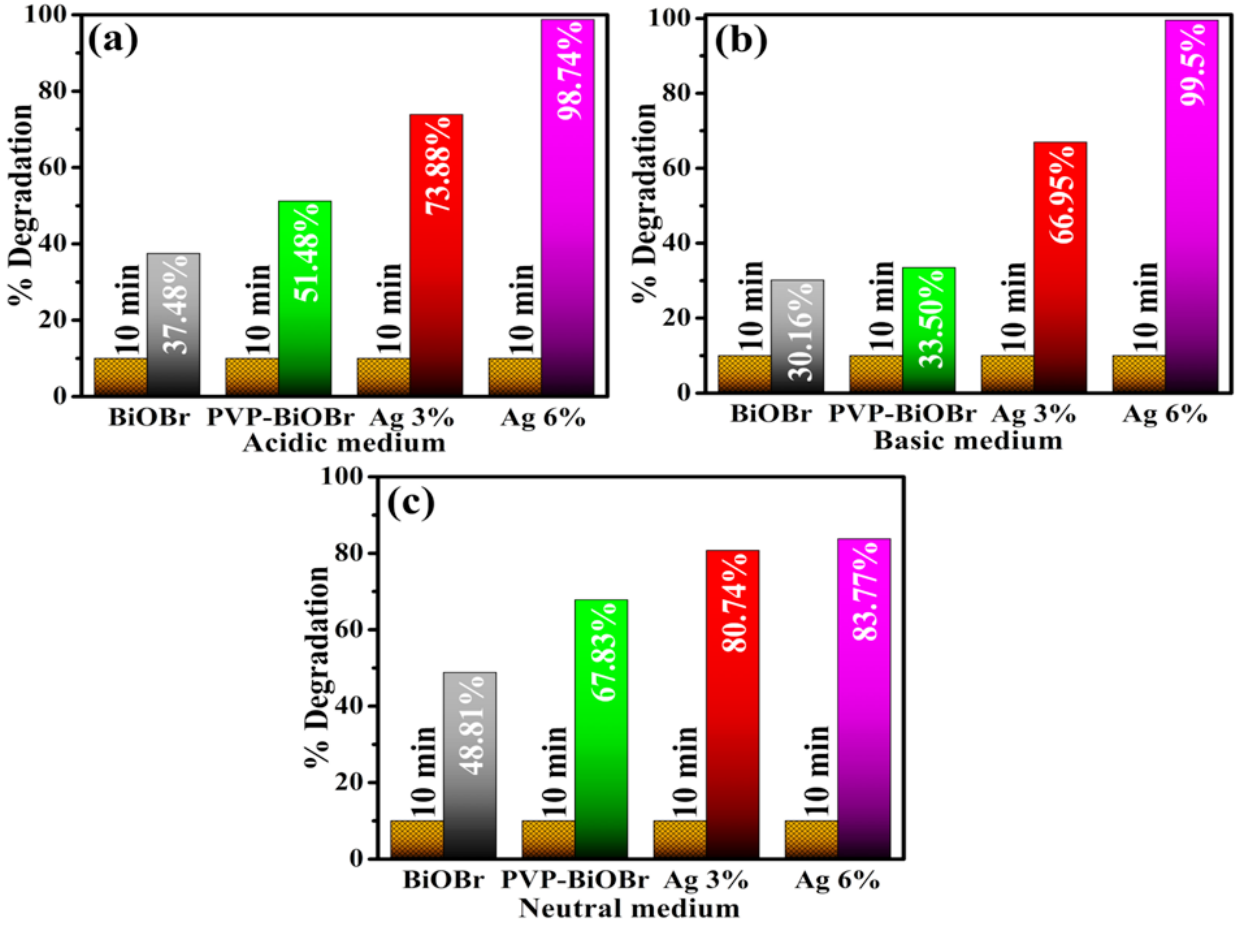

Fig. 5: Catalytic activity of pristine and Ag/PVP-doped BiOBr QDs in (a) acidic, (b) basic, and (c) neutral media

Table 1. Comparison of the catalytic activity of Ag/PVP doped BiOBr

Catalysts	Synthesis method	Targeted dye	Degradation efficacy (%)	Ref.

Reduced graphene-BiOBr	Co-precipitation method	Rhodamine B (RhB) (light)	>95	[53]
g-C_3N_4-BiOBr composite	Hydrothermal	RhB (light)	94	[54]
BiOBr/$Bi_{24}O_{31}Br_{10}$/TiO_2	Hydrothermal	RhB (light)	78	[55]
Graphene oxide–BiOBr	Hydrothermal	RhB (light)	95	[56]
BiOBr microsphere	Solvothermal	Methyl orange	50	[57]
SnS_2-BiOBr	hydrothermal	RhB (light)	88	[58]
$BiVO_4$-BiOBr	Sol gel	RhB (light)	90	[59]
6% Ag/PVP-BiOBr	Co-precipitation	MB	99	Present study

The bactericidal effectiveness of both un-doped and doped BiOBr was determined through a well-diffusion investigation, which involved evaluating the inhibition zones as a measure of antimicrobial activity. At both minimum and maximum dosages, there were detectable inhibition areas ranging from (0.95 – 3.10 mm) to (1.90 – 4.95 mm) for MDR *E. coli*, Table 2. The effectiveness against MDR *E. coli* improved from 46.1% to 66.8% and towards Ag/PVP-BiOBr QDs, from 47.8% to 68.2% at the minimum and maximum concentrations, respectively, as illustrated in Fig. S5(a-b). Ag/PVP doped BiOBr at 6 wt% doping showed significant

antibacterial action against MDR *E. coli* in contrast to the 7.25 mm and 0 mm inhibition radius of +ve and -ve controls.

To suppress microbiological organisms, to stop cell reproduction, QDs primarily exploit three molecular pathways: destroying cell walls and membranes, creating reactive oxygen species (ROS), and anchoring genetic content (DNA/RNA). Polymers have indeed been added to QDs to strengthen their adhesion towards bacterial components and boost their ROS generation [60], as illustrated in Fig. S6. The antibacterial effectiveness is inversely related to the material's size [61]. Bacteria are killed when their membranes are breached by the production of reactive oxygen species from the breakdown of tiny particles. [62,63]. The antibacterial activity of Bi^{3+} is enhanced when it is distributed sufficiently inside the bacterial cells because it affects bacterial membrane stability and prevents the development of biofilms [63].

Table 2 Antibacterial efficacy of BiOBr and Ag/PVP-doped BiOBr QDs

		MDR *E. coli* Inhibition region (mm)		
Samples	0.5 mg/50 µL	1.0 mg/50 µL	Ciprofloxacin +ve control	DI water -ve control
BiOBr	0.95	1.90	7.25	0
PVP-BiOBr	1.55	2.05	7.25	0
Ag 3%	2.60	3.35	7.25	0
Ag 6%	3.10	4.95	7.25	0

Molecular docking study

Computational methods, especially molecular docking studies, have received much attention over the last several decades since they allow for a comprehensive exploration of the mechanisms underpinning a wide range of biological activities. This research used molecular docking to identify enzyme inhibitors based on QDs binding and inhibitory potential. Significant targets for antibiotics discovery include the bacterial enzymes FabH and DNA gyrase, required for the survival and multiplication of bacteria [64,65]. The docking scores of both PVP-doped BiOBr QDs and Ag/PVP-doped BiOBr QDs were analyzed. With a binding score of 3.77, the best-docked conformation of PVP-doped BiOBr QDs demonstrated H-bonding interactions with Thr165 and Asn46 and pi-alkyl interactions with Ile78, Met95, and Asn120 for DNA gyrase (Fig. 6(a-b)). Whereas Ag/PVP-doped BiOBr QDs exhibited pi-alkyl interaction with Ile78 and Pro79 having a docking score of 7.47, H-interaction was seen with Gly72, Asp73, Gly77, and Thr165 (Fig. 6(c-d)).

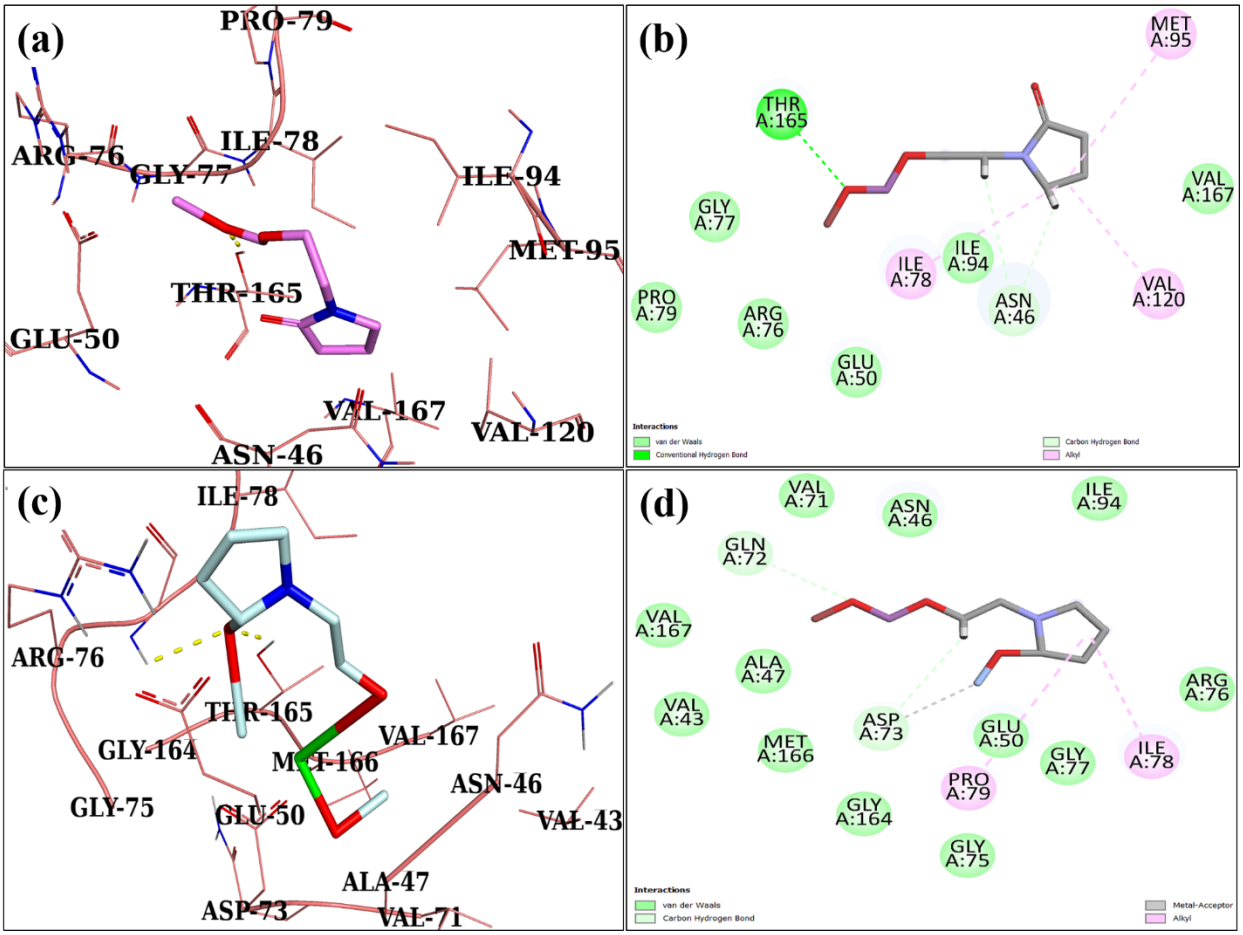

Fig. 6: Binding interaction pattern within the active domain of *E. coli* DNA gyrase. (a) & (b) show the interaction pattern and a 2D view of PVP-doped BiOBr inside the FabH binding site, respectively. (c) & (d) demonstrated the binding mode (3D and 2D) of the Ag/PVP-doped BiOBr at the DNA gyrase active center.

For FabH, an additional striking target for antibiotic discovery, PVP-doped BiOBr QDs unveiled a strong binding propensity with binding site residues having a binding score of 4.78, where PVP-doped BiOBr exhibited H-bonding with Thr81 and Leu201 and pi-alkyl interactions with Leu189, Leu191, and Leu205 (Fig. 7(a-b)). Although the best-docked conformation of Ag/PVP-doped BiOBr QDs displayed H-bonding interactions with Thr81, Ser276, and Gly306, and pi-

alkyl interactions with Leu189, Leu191, and Leu205, with a binding score of 5.24, H-bonding interactions were also seen with Leu189, Leu191, and Leu205 (Fig. 7(c-d)). In silico antibacterial activities are equivalent to in-vitro antimicrobial activities, suggesting that Ag/PVP-doped BiOBr QDs are potential inhibitors for FabH and DNA gyrase from *E. coli*, *requiring* additional investigation.

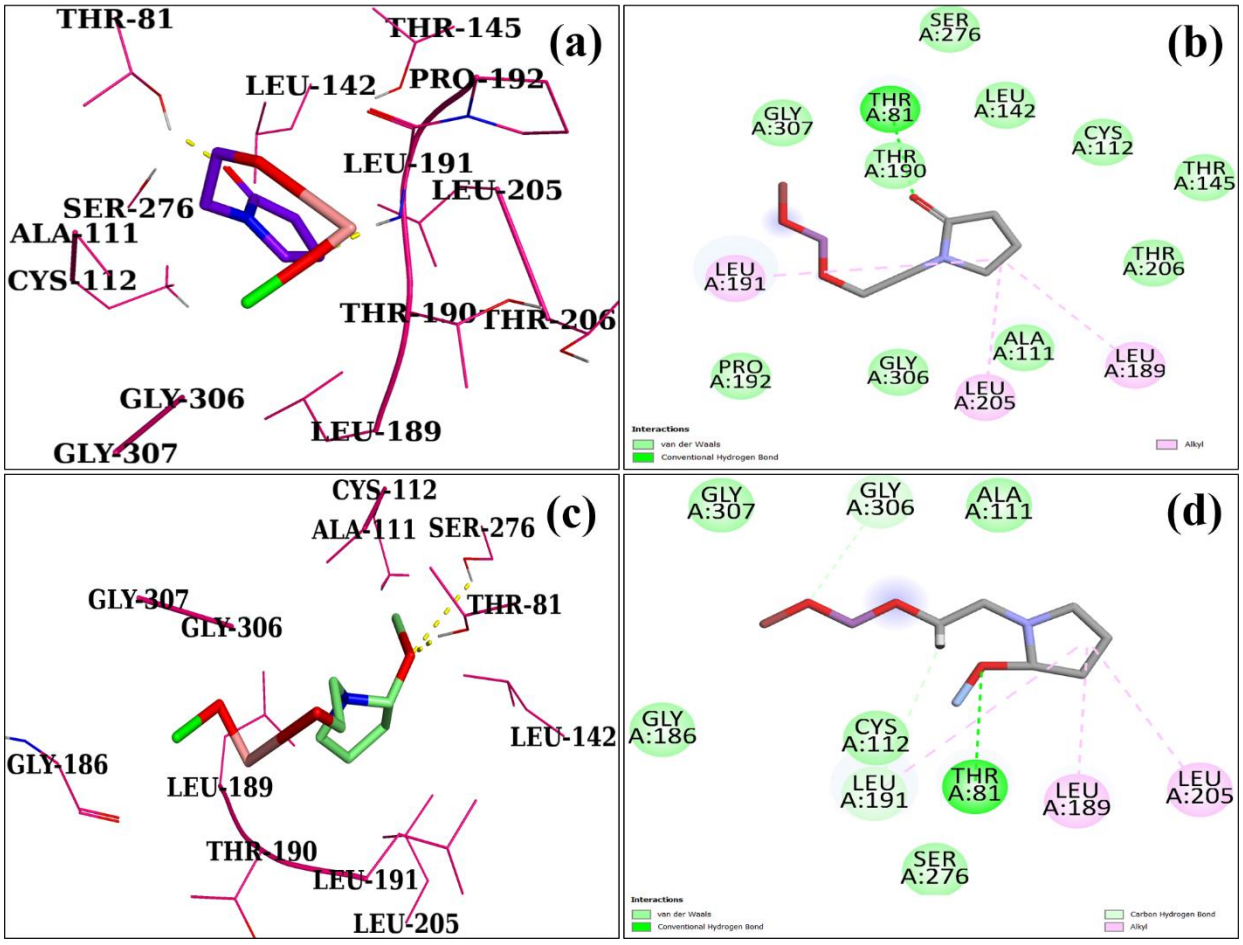

Fig. 7: Binding interaction pattern within the active region of *E. coli* FabH. (a) & (b) show the interaction pattern and a 2D view of PVP-doped BiOBr inside the FabH binding site, respectively. (c) & (d) demonstrated the binding mode (3D and 2D) of the Ag/PVP-doped BiOBr at the FabH active center.

4. CONCLUSION

This study successfully prepared BiOBr and Ag (3 and 6 wt. %) Ag/PVP-doped BiOBr QDs using a low-cost co-precipitation method. XRD spectra affirmed the tetragonal structure of BiOBr QDs, and a decrease in crystallinity was observed upon Ag and PVP doping. TEM images exhibited cluster BiOBr QDs formation and reduced particle size by adding Ag and PVP. UV-Vis spectroscopy revealed a blue shift in the absorption spectra that caused to increase in E_g upon doping. The catalytic activity signified maximum degradation of MB dye up to 83.77% in neutral, 98.74% in acidic, and 99.5% in alkaline environments. In particular, doped BiOBr QDs have shown potent bactericidal activity towards pathogenic etiologic agents like MDR *E. coli*. Molecular docking analyses demonstrated that Ag/PVP-doped BiOBr QDs from *E. coli* might potentially block the FabH and DNA gyrase enzymes. Consequently, BiOBr QDs may be cost-efficient, environmentally benign, and efficacious against bacteria and industrial dye degraders.

Acknowledgment: The authors thank HEC, Pakistan, through NRPU-20-17615 (Dr. M. Ikram). This research was funded by the Princess Nourah bint Abdulrahman University Researchers Supporting Project number (PNURSP2023R7), Princess Nourah bint Abdulrahman University, Riyadh, Saudi Arabia. The authors extend their appreciation to the Deanship of Scientific Research at King Khalid University, Saudi Arabia for funding this work through Large Groups Project under grant number L.R.G.P2/516/44.

Conflict of Interest: This manuscript is free from any known conflict of interest

Data Availability Statement: On demand

REFERENCES:

[1] Z. Wang, A. Wu, L.C. Ciacchi, G. Wei, Recent advances in Nanoporous Membranes for

Water Purification, Nanomaterials. 8 (2018). https://doi.org/10.3390/nano8020065.

[2] M.E. Mahmoud, N.A. Fekry, A.M. Abdelfattah, A novel nanobiosorbent of functionalized graphene quantum dots from rice husk with barium hydroxide for microwave enhanced removal of lead (II) and lanthanum (III), Bioresour. Technol. 298 (2020) 122514. https://doi.org/10.1016/j.biortech.2019.122514.

[3] E. Brillas, C.A. Martínez-Huitle, Decontamination of wastewaters containing synthetic organic dyes by electrochemical methods. An updated review, Appl. Catal. B Environ. 166–167 (2015) 603–643. https://doi.org/10.1016/j.apcatb.2014.11.016.

[4] G.O. El-Sayed, Removal of methylene blue and crystal violet from aqueous solutions by palm kernel fiber, Desalination. 272 (2011) 225–232. https://doi.org/10.1016/j.desal.2011.01.025.

[5] S. Moeen, M. Ikram, A. Haider, J. Haider, A. Ul-Hamid, W. Nabgan, T. Shujah, M. Naz, I. Shahzadi, Comparative Study of Sonophotocatalytic, Photocatalytic, and Catalytic Activities of Magnesium and Chitosan-Doped Tin Oxide Quantum Dots, ACS Omega. 7 (2022) 46428–46439. https://doi.org/10.1021/ACSOMEGA.2C05133.

[6] R.A. Kristanti, M.K.A. Kamisan, T. Hadibarata, Treatability of Methylene Blue Solution by Adsorption Process Using Neobalanocarpus hepmii and Capsicum annuum, Water. Air. Soil Pollut. 227 (2016). https://doi.org/10.1007/s11270-016-2834-y.

[7] K. Naseem, Z.H. Farooqi, M.Z. Ur Rehman, M.A. Ur Rehman, R. Begum, R. Huma, A. Shahbaz, J. Najeeb, A. Irfan, A systematic study for removal of heavy metals from aqueous media using sorghum bicolor: An efficient biosorbent, Water Sci. Technol. 77

(2018) 2355–2368. https://doi.org/10.2166/wst.2018.190.

[8] R. Begum, J. Najeeb, A. Sattar, K. Naseem, A. Irfan, A.G. Al-Sehemi, Z.H. Farooqi, Chemical reduction of methylene blue in the presence of nanocatalysts: A critical review, Rev. Chem. Eng. 36 (2020) 749–770. https://doi.org/10.1515/revce-2018-0047.

[9] N.U. Barambu, M.R. Bilad, L. Marbelia, N. Arahman, Gravity-driven membrane filtration for decentralized water and wastewater treatment, in: Water Eng. Model. Math. Tools, 2021: pp. 177–185. https://doi.org/10.1016/B978-0-12-820644-7.00025-6.

[10] C.M.B. Neves, O.M.S. Filipe, N. Mota, S.A.O. Santos, A.J.D. Silvestre, E.B.H. Santos, M.G.P.M.S. Neves, M.M.Q. Simões, Photodegradation of metoprolol using a porphyrin as photosensitizer under homogeneous and heterogeneous conditions, J. Hazard. Mater. 370 (2019) 13–23. https://doi.org/10.1016/j.jhazmat.2018.11.055.

[11] A. Bashir, L.A. Malik, S. Ahad, T. Manzoor, M.A. Bhat, G.N. Dar, A.H. Pandith, Removal of heavy metal ions from aqueous system by ion-exchange and biosorption methods, Environ. Chem. Lett. 17 (2019) 729–754. https://doi.org/10.1007/s10311-018-00828-y.

[12] S. Xu, H. Bi, G. Liu, B. Su, Integration of catalytic ozonation and adsorption processes for increased efficiency of textile wastewater treatment, Water Environ. Res. 91 (2019) 650–660. https://doi.org/10.1002/wer.1102.

[13] S. Saghafi, A. Ebrahimi, N. Mehrdadi, G.N. Bidhendy, Evaluation of aerobic/anaerobic industrial wastewater treatment processes: The application of multi-criteria decision analysis, Environ. Prog. Sustain. Energy. 38 (2019). https://doi.org/10.1002/ep.13166.

[14] M. Nasrollahzadeh, Z. Issaabadi, S.M. Sajadi, Green synthesis of a Cu/MgO nanocomposite by: Cassytha filiformis L. extract and investigation of its catalytic activity in the reduction of methylene blue, congo red and nitro compounds in aqueous media, RSC Adv. 8 (2018) 3723–3735. https://doi.org/10.1039/c7ra13491f.

[15] R. Dou, H. Cheng, J. Ma, S. Komarneni, Manganese doped magnetic cobalt ferrite nanoparticles for dye degradation via a novel heterogeneous chemical catalysis, Mater. Chem. Phys. 240 (2020). https://doi.org/10.1016/j.matchemphys.2019.122181.

[16] G. Karthigadevi, S. Manikandan, N. Karmegam, R. Subbaiya, S. Chozhavendhan, B. Ravindran, S.W. Chang, M.K. Awasthi, Chemico-nanotreatment methods for the removal of persistent organic pollutants and xenobiotics in water – A review, Bioresour. Technol. 324 (2021) 124678. https://doi.org/10.1016/j.biortech.2021.124678.

[17] F. Gomes, M. Henriques, Control of Bovine Mastitis: Old and Recent Therapeutic Approaches, Curr. Microbiol. 72 (2016) 377–382. https://doi.org/10.1007/s00284-015-0958-8.

[18] A. Chwalibog, E. Sawosz, A. Hotowy, J. Szeliga, S. Mitura, K. Mitura, M. Grodzik, P. Orlowski, A. Sokolowska, Visualization of interaction between inorganic nanoparticles and bacteria or fungi, Int. J. Nanomedicine. 5 (2010) 1085–1094. https://doi.org/10.2147/IJN.S13532.

[19] F. Liu, J.H. Yang, J. Zuo, D. Ma, L. Gan, B. Xie, P. Wang, B. Yang, Graphene-supported nanoscale zero-valent iron: Removal of phosphorus from aqueous solution and mechanistic study, J. Environ. Sci. (China). 26 (2014) 1751–1762. https://doi.org/10.1016/j.jes.2014.06.016.

[20] Z. Li, S. Zhang, B. Omar Mohammed, An efficient three-level nano-design for reversible gate using quantum dot-cellular automata with cost analysis, Mater. Sci. Eng. B Solid-State Mater. Adv. Technol. 294 (2023) 116526. https://doi.org/10.1016/j.mseb.2023.116526.

[21] X. Hu, L. Cheng, G. Li, One-pot hydrothermal fabrication of basic bismuth nitrate/BiOBr composite with enhanced photocatalytic activity, Mater. Lett. 203 (2017) 77–80. https://doi.org/10.1016/j.matlet.2017.05.123.

[22] S. Luo, F. Qin, Y. Ming, H. Zhao, Y. Liu, R. Chen, Fabrication uniform hollow Bi2S3 nanospheres via Kirkendall effect for photocatalytic reduction of Cr(VI) in electroplating industry wastewater, J. Hazard. Mater. 340 (2017) 253–262. https://doi.org/10.1016/j.jhazmat.2017.06.044.

[23] Y. Guo, Y. Zhang, N. Tian, H. Huang, Homogeneous {001}-BiOBr/Bi heterojunctions: Facile controllable synthesis and morphology-dependent photocatalytic activity, ACS Sustain. Chem. Eng. 4 (2016) 4003–4012. https://doi.org/10.1021/acssuschemeng.6b00884.

[24] Y. Hou, Y. Gan, Z. Yu, X. Chen, L. Qian, B. Zhang, L. Huang, J. Huang, Solar promoted azo dye degradation and energy production in the bio-photoelectrochemical system with a g-C3N4/BiOBr heterojunction photocathode, J. Power Sources. 371 (2017) 26–34. https://doi.org/10.1016/j.jpowsour.2017.10.033.

[25] H. Huang, X. Han, X. Li, S. Wang, P.K. Chu, Y. Zhang, Fabrication of multiple heterojunctions with tunable visible-light-active photocatalytic reactivity in BiOBr-BiOI full-range composites based on microstructure modulation and band structures, ACS Appl.

Mater. Interfaces. 7 (2015) 482–492. https://doi.org/10.1021/am5065409.

[26] C. Guo, Y. He, P. Du, X. Zhao, J. Lv, W. Meng, Y. Zhang, J. Xu, Novel magnetically recoverable BiOBr/iron oxides heterojunction with enhanced visible light-driven photocatalytic activity, Appl. Surf. Sci. 320 (2014) 383–390. https://doi.org/10.1016/j.apsusc.2014.09.111.

[27] A.L. Desa, N.H.H. Hairom, D.A.B. Sidik, N. Misdan, N. Yusof, M.K. Ahmad, A.W. Mohammad, A comparative study of ZnO-PVP and ZnO-PEG nanoparticles activity in membrane photocatalytic reactor (MPR) for industrial dye wastewater treatment under different membranes, J. Environ. Chem. Eng. 7 (2019). https://doi.org/10.1016/j.jece.2019.103143.

[28] J. Pan, Y. Li, G. Guo, X. Zhao, J. Yu, Z. Li, S. Xu, B. Man, D. Wei, C. Zhang, Synergizing piezoelectric and plasmonic modulation of PVDF/MoS2 cavity/Au for enhanced photocatalysis, Appl. Surf. Sci. 577 (2022). https://doi.org/10.1016/j.apsusc.2021.151811.

[29] P.P. Gotipamul, G. Vattikondala, K.D. Rajan, S. Khanna, M. Rathinam, S. Chidambaram, Impact of piezoelectric effect on the heterogeneous visible photocatalysis of g-C3N4/Ag/ZnO tricomponent, Chemosphere. 287 (2022). https://doi.org/10.1016/j.chemosphere.2021.132298.

[30] F. Fu, J. Gu, J. Cao, R. Shen, H. Liu, Y. Zhang, X. Liu, J. Zhou, Reduction of Silver Ions Using an Alkaline Cellulose Dope: Straightforward Access to Ag/ZnO Decorated Cellulose Nanocomposite Film with Enhanced Antibacterial Activities, ACS Sustain. Chem. Eng. 6 (2018) 738–748. https://doi.org/10.1021/acssuschemeng.7b03059.

[31] R. Subbaiya, M. Saravanan, A.R. Priya, K.R. Shankar, M. Selvam, M. Ovais, R. Balajee, H. Barabadi, Biomimetic synthesis of silver nanoparticles from Streptomyces atrovirens and their potential anticancer activity against human breast cancer cells, IET Nanobiotechnology. 11 (2017) 965–972. https://doi.org/10.1049/iet-nbt.2016.0222.

[32] A. Raza, J.Z. Hassan, M. Ikram, S. Naz, A. Haider, A. Ul-Hamid, I. Shahzadi, J. Haider, S. Goumri-Said, M.B. Kanoun, S. Ali, Molecular docking and DFT analyses of magnetic cobalt doped MoS2 and BN nanocomposites for catalytic and antimicrobial explorations, Surfaces and Interfaces. 27 (2021). https://doi.org/10.1016/j.surfin.2021.101571.

[33] F. Ali, S.B. Khan, T. Kamal, K.A. Alamry, A.M. Asiri, T.R.A. Sobahi, Chitosan coated cotton cloth supported zero-valent nanoparticles: Simple but economically viable, efficient and easily retrievable catalysts, Sci. Rep. 7 (2017). https://doi.org/10.1038/s41598-017-16815-2.

[34] D.C. McKinney, C.J. Eyermann, R.F. Gu, J. Hu, S.L. Kazmirski, S.D. Lahiri, A.R. McKenzie, A.B. Shapiro, G. Breault, Antibacterial FabH Inhibitors with Mode of Action Validated in Haemophilus influenzae by in Vitro Resistance Mutation Mapping, ACS Infect. Dis. 2 (2016) 456–464. https://doi.org/10.1021/acsinfecdis.6b00053.

[35] F. Ushiyama, H. Amada, T. Takeuchi, N. Tanaka-Yamamoto, H. Kanazawa, K. Nakano, M. Mima, A. Masuko, I. Takata, K. Hitaka, K. Iwamoto, H. Sugiyama, N. Ohtake, Lead Identification of 8-(Methylamino)-2-oxo-1,2-dihydroquinoline Derivatives as DNA Gyrase Inhibitors: Hit-to-Lead Generation Involving Thermodynamic Evaluation, ACS Omega. 5 (2020) 10145–10159. https://doi.org/10.1021/acsomega.0c00865.

[36] M. Ikram, K. Chaudhary, A. Shahzadi, A. Haider, I. Shahzadi, A. Ul-Hamid, N. Abid, J.

Haider, W. Nabgan, A.R. Butt, Chitosan/starch-doped MnO2 nanocomposite served as dye degradation, bacterial activity, and insilico molecular docking study, Mater. Today Nano. 20 (2022). https://doi.org/10.1016/j.mtnano.2022.100271.

[37] I. Shahzadi, M. Islam, H. Saeed, A. Haider, A. Shahzadi, J. Haider, N. Ahmed, A. Ul-Hamid, W. Nabgan, M. Ikram, H.A. Rathore, Formation of biocompatible MgO/cellulose grafted hydrogel for efficient bactericidal and controlled release of doxorubicin, Int. J. Biol. Macromol. 220 (2022) 1277–1286. https://doi.org/10.1016/j.ijbiomac.2022.08.142.

[38] I. Shahzadi, M. Islam, H. Saeed, A. Shahzadi, J. Haider, A. Haider, M. Imran, H.A. Rathore, A. Ul-Hamid, W. Nabgan, M. Ikram, Facile synthesis of copolymerized cellulose grafted hydrogel doped calcium oxide nanocomposites with improved antioxidant activity for anti-arthritic and controlled release of doxorubicin for anti-cancer evaluation., Int. J. Biol. Macromol. 235 (2023) 123874. https://doi.org/10.1016/j.ijbiomac.2023.123874.

[39] X. Zhang, P. Yang, B. Yang, Y. Bai, W. Liu, K. Zhang, Synthesis of the composite catalyst Bi4O5Br2/BiOBr for the improved photocatalytic degradation of oilfield produced wastewater, J. Mater. Sci. Mater. Electron. 30 (2019) 17276–17287. https://doi.org/10.1007/s10854-019-02074-6.

[40] Ayesha, M. Imran, A. Haider, I. Shahzadi, S. Moeen, A. Ul-Hamid, W. Nabgan, A. Shahzadi, T. Alshahrani, M. Ikram, Polyvinylpyrrolidone and chitosan-coated magnetite (Fe3O4) nanoparticles for catalytic and antimicrobial activity with molecular docking analysis, J. Environ. Chem. Eng. 11 (2023) 110088. https://doi.org/10.1016/j.jece.2023.110088.

[41] N. Susha, K. Nandakumar, S.S. Nair, Enhanced photoconductivity in CdS/betanin

composite nanostructures, RSC Adv. 8 (2018) 11330–11337. https://doi.org/10.1039/c7ra13116j.

[42] Z.S. Liu, J.L. Liu, H.Y. Wang, G. Cao, J.N. Niu, Boron-doped bismuth oxybromide microspheres with enhanced surface hydroxyl groups: Synthesis, characterization and dramatic photocatalytic activity, J. Colloid Interface Sci. 463 (2016) 324–331. https://doi.org/10.1016/j.jcis.2015.10.028.

[43] B. Li, W. Xu, D. Kronlund, A. Määttänen, J. Liu, J.H. Smått, J. Peltonen, S. Willför, X. Mu, C. Xu, Cellulose nanocrystals prepared via formic acid hydrolysis followed by TEMPO-mediated oxidation, Carbohydr. Polym. 133 (2015) 605–612. https://doi.org/10.1016/j.carbpol.2015.07.033.

[44] X. jing Wang, Q. Wang, F. tang Li, W. yan Yang, Y. Zhao, Y. juan Hao, S. jun Liu, Novel BiOCl-C3N4 heterojunction photocatalysts: In situ preparation via an ionic-liquid-assisted solvent-thermal route and their visible-light photocatalytic activities, Chem. Eng. J. 234 (2013) 361–371. https://doi.org/10.1016/j.cej.2013.08.112.

[45] L. Ye, L. Tian, T. Peng, L. Zan, Synthesis of highly symmetrical BiOI single-crystal nanosheets and their {001} facet-dependent photoactivity, J. Mater. Chem. 21 (2011) 12479–12484. https://doi.org/10.1039/c1jm11005e.

[46] S. Asadzadeh-Khaneghah, A. Habibi-Yangjeh, K. Nakata, Graphitic carbon nitride nanosheets anchored with BiOBr and carbon dots: Exceptional visible-light-driven photocatalytic performances for oxidation and reduction reactions, J. Colloid Interface Sci. 530 (2018) 642–657. https://doi.org/10.1016/j.jcis.2018.07.024.

[47] M.C. Sportelli, R.A. Picca, M. Izzi, N. Cioffi, Green Synthesis and Analytical Characterization of Core-Shell Copper Sub-Microparticles, Chem. - A Eur. J. 29 (2023) e202203510. https://doi.org/10.1002/chem.202203510.

[48] C. Gong, J. Chu, S. Qian, C. Yin, X. Hu, H. Wang, Y. Wang, X. Ding, S. Jiang, A. Li, Y. Gong, X. Wang, C. Li, T. Zhai, J. Xiong, Large-Scale Ultrathin 2D Wide-Bandgap BiOBr Nanoflakes for Gate-Controlled Deep-Ultraviolet Phototransistors, Adv. Mater. 32 (2020). https://doi.org/10.1002/adma.201908242.

[49] T. Senasu, T. Chankhanittha, K. Hemavibool, S. Nanan, Solvothermal synthesis of BiOBr photocatalyst with an assistant of PVP for visible-light-driven photocatalytic degradation of fluoroquinolone antibiotics, Catal. Today. 384–386 (2022) 209–227. https://doi.org/10.1016/j.cattod.2021.04.008.

[50] Y. Yan, H. Yang, Z. Yi, X. Wang, R. Li, T. Xian, Evolution of Bi Nanowires from BiOBr Nanoplates through a NaBH4 Reduction Method with Enhanced Photodegradation Performance, Environ. Eng. Sci. 37 (2020) 64–77. https://doi.org/10.1089/ees.2019.0284.

[51] B. Zhang, M. Zhang, L. Zhang, P.A. Bingham, W. Li, S. Kubuki, PVP surfactant-modified flower-like BiOBr with tunable bandgap structure for efficient photocatalytic decontamination of pollutants, Appl. Surf. Sci. 530 (2020). https://doi.org/10.1016/j.apsusc.2020.147233.

[52] M. Ikram, S. Hayat, M. Imran, A. Haider, S. Naz, A. Ul-Hamid, I. Shahzadi, J. Haider, A. Shahzadi, W. Nabgan, S. Ali, Novel Ag/cellulose-doped CeO2 quantum dots for efficient dye degradation and bactericidal activity with molecular docking study, Carbohydr. Polym. 269 (2021). https://doi.org/10.1016/j.carbpol.2021.118346.

[53] A.M. Alansi, M. Al-Qunaibit, I.O. Alade, T.F. Qahtan, T.A. Saleh, Visible-light responsive BiOBr nanoparticles loaded on reduced graphene oxide for photocatalytic degradation of dye, J. Mol. Liq. 253 (2018) 297–304. https://doi.org/10.1016/j.molliq.2018.01.034.

[54] M. Jiang, Y. Shi, J. Huang, L. Wang, H. She, J. Tong, B. Su, Q. Wang, Synthesis of Flowerlike g-C3N4/BiOBr with Enhanced Visible Light Photocatalytic Activity for Dye Degradation, Eur. J. Inorg. Chem. 2018 (2018) 1834–1841. https://doi.org/10.1002/ejic.201800110.

[55] S.R. Zhu, M.K. Wu, W.N. Zhao, F.Y. Yi, K. Tao, L. Han, Fabrication of heterostructured BiOBr/Bi24O31Br10/TiO2 photocatalyst by pyrolysis of MOF composite for dye degradation, J. Solid State Chem. 255 (2017) 17–26. https://doi.org/10.1016/j.jssc.2017.07.038.

[56] S. Vadivel, M. Vanitha, A. Muthukrishnaraj, N. Balasubramanian, Graphene oxide-BiOBr composite material as highly efficient photocatalyst for degradation of methylene blue and rhodamine-B dyes, J. Water Process Eng. 1 (2014) 17–26. https://doi.org/10.1016/j.jwpe.2014.02.003.

[57] A.C. Mera, H. Váldes, F.J. Jamett, M.F. Meléndrez, BiOBr microspheres for photocatalytic degradation of an anionic dye, Solid State Sci. 65 (2017) 15–21. https://doi.org/10.1016/j.solidstatesciences.2017.01.001.

[58] F. Qiu, W. Li, F. Wang, H. Li, X. Liu, J. Sun, In-situ synthesis of novel Z-scheme SnS2/BiOBr photocatalysts with superior photocatalytic efficiency under visible light, J. Colloid Interface Sci. 493 (2017) 1–9. https://doi.org/10.1016/j.jcis.2016.12.066.

[59] S. Liu, J. Chen, D. Liu, L. Shan, X. Zhang, Improved visible light photocatalytic performance through an in situ composition-transforming synthesis of BiVO4/BiOBr photocatalyst, J. Nanoparticle Res. 21 (2019) 1–10. https://doi.org/10.1007/s11051-019-4625-z.

[60] K. Rajendiran, Z. Zhao, D.S. Pei, A. Fu, Antimicrobial activity and mechanism of functionalized quantum dots, Polymers (Basel). 11 (2019). https://doi.org/10.3390/polym11101670.

[61] A. Haider, M. Ijaz, M. Imran, M. Naz, H. Majeed, J.A. Khan, M.M. Ali, M. Ikram, Enhanced bactericidal action and dye degradation of spicy roots' extract-incorporated fine-tuned metal oxide nanoparticles, Appl. Nanosci. 10 (2020) 1095–1104. https://doi.org/10.1007/s13204-019-01188-x.

[62] W. Fang, X. Chaofa, J. Zheng, G. Chen, K. Jiang, Fabrication of Cu-Ag bimetal nanotube-based copper silicates for enhancement of antibacterial activities, RSC Adv. 5 (2015) 39612–39619. https://doi.org/10.1039/c5ra06065f.

[63] U. Qumar, M. Ikram, M. Imran, A. Haider, A. Ul-Hamid, J. Haider, K.N. Riaz, S. Ali, Synergistic effect of Bi-doped exfoliated MoS2 nanosheets on their bactericidal and dye degradation potential, Dalt. Trans. 49 (2020) 5362–5377. https://doi.org/10.1039/d0dt00924e.

[64] S. McAuley, A. Huynh, A. Howells, C. Walpole, A. Maxwell, J.R. Nodwell, Discovery of a Novel DNA Gyrase-Targeting Antibiotic through the Chemical Perturbation of Streptomyces venezuelae Sporulation, Cell Chem. Biol. 26 (2019) 1274--1282.e4. https://doi.org/10.1016/j.chembiol.2019.06.002.

[65] P. V Adrian, K.P. Klugman, Mutations in the dihydrofolate reductase gene of trimethoprim-resistant isolates of Streptococcus pneumoniae, Antimicrob. Agents Chemother. 41 (1997) 2406–2413. https://doi.org/10.1128/aac.41.11.2406.